Nano Energy 33 (2017) 293–305

Contents lists available at ScienceDirect

Nano Energy

journal homepage: www.elsevier.com/locate/nanoen

Full paper

Highly active nanostructured palladium-ceria electrocatalysts for the hydrogen oxidation reaction in alkaline medium

Hamish A. Miller[a,*], Francesco Vizza[a,*], Marcello Marelli[b], Anicet Zadick[c,d], Laetitia Dubau[c,d], Marian Chatenet[c,d,e], Simon Geiger[f], Serhiy Cherevko[f,g], Huong Doan[h], Ryan K. Pavlicek[h], Sanjeev Mukerjee[h], Dario R. Dekel[i,j,*]

[a] Istituto di Chimica dei Composti Organometallici (CNR-ICCOM), via Madonna del Piano 10, 50019 Sesto Fiorentino, Firenze, Italy
[b] Istituto di Scienze e Tecnologie Molecolari (ISTM-CNR), via Camillo Golgi 19, 20133 Milano, Italy
[c] University of Grenoble Alpes, LEPMI, F-38000 Grenoble, France
[d] CNRS, LEPMI, F-38000 Grenoble, France
[e] French University Institute (IUF), Paris, France
[f] Department of Interface Chemistry and Surface Engineering, Max-Planck-Institut für Eisenforschung GmbH, 40237 Düsseldorf, Germany
[g] Helmholtz-Institute Erlangen-Nürnberg for Renewable Energy (IEK-11), Forschungszentrum Jülich, 91058 Erlangen, Germany
[h] Department of Chemistry and Chemical Biology, Northeastern University, Boston, MA, 02115, USA
[i] The Wolfson Department of Chemical Engineering, Technion – Israel Institute of Technology, Haifa 3200003, Israel
[j] The Nancy & Stephan Grand Technion Energy Program (GTEP), Technion – Israel Institute of Technology, Haifa 3200003, Israel

ARTICLE INFO

Keywords:
Fuel cell
Platinum free
Anion exchange membrane
Palladium
Ceria, hydrogen oxidation

ABSTRACT

We report an interesting new class of bifunctional electrocatalysts, Pd/C-CeO_2, with excellent activity and stability for the hydrogen oxidation reaction (HOR) under alkaline conditions. The unique structure of palladium deposited onto a mixed support of Vulcan XC-72 carbon and CeO_2 consists of Pd metal preferable deposited on the ceria regions of the catalyst. The CeO_2-Pd interaction leads to enhanced HOR kinetics and increased stability. Here we compare catalysts with three different Pd loadings and show that the 10 wt% Pd sample has optimized activity. Hydrogen pumping and fuel cell experiments based on this catalyst show higher activities as compared to a Pd/C sample without ceria. Metal dissolution tests and identical location transmission microscopy experiments show that the catalyst stability under harsh potential cycling experiments in alkaline medium is significantly improved as compared to Pd/C, making this material one of the best options for use as highly active and highly stable electrocatalysts for the HOR in anion exchange membrane fuel cells.

1. Introduction

Anion exchange membrane fuel cells (AEM-FCs) have received increasing attention as this technology has the potential to replace expensive platinum and platinum alloy materials currently used in fuel cell electrodes, significantly reducing the cost of fuel cell devices [1]. Recently, significant progress has been made in improving material components for AEM-FCs in particular cell hardware, membranes, ionomers and cathode catalysts for the oxygen reduction reaction (ORR) [2–16]. However, the sluggish hydrogen oxidation reaction (HOR) kinetics of electrocatalysts under alkaline conditions have limited the development of affordable Pt-free catalysts and AEM-FC technology is still awaiting new advanced catalytic materials to fulfill its potential [17]. Hence, the realization of a completely Pt-free AEM-FC requires the development of novel anode catalyst structures that enhance the HOR of the supported metal nanoparticles (NPs) [18]. A new class of Pd based materials that exploit mixed carbon and metal oxide supports has recently been reported that have led for the first time, to performances of non-Pt AEM-FCs with power densities around 0.5 W cm^{-2}, operating with partially filtered air at the cathode and dry hydrogen at the anode [19]. In particular, the addition of CeO_2 to Vulcan XC-72 carbon with a 50:50 weight ratio yields a conductive support onto which Pd deposits preferentially onto the ceria regions (confirmed by EDX-STEM and XAS investigations) [19]. When compared to a Pd supported on carbon catalyst (without ceria) with the same particle size distribution and metal loading, a 5-fold improvement is obtained in the anode performance under the same fuel cell conditions for the Pd/C-CeO_2 catalyst. It is believed that the presence of an intimate contact between ceria and Pd enhances the OH^- transfer from the anion conducting membrane and ionomer regions of the fuel

* Corresponding authors.
E-mail address: hamish.miller@iccom.cnr.it (H.A. Miller).

http://dx.doi.org/10.1016/j.nanoen.2017.01.051
Received 25 November 2016; Received in revised form 18 January 2017; Accepted 24 January 2017
Available online 26 January 2017

cell to the metal surface where the HOR takes place [20]. Cyclic voltammetry (CV) studies have shown a weakening of the Pd-H bonding when ceria is in contact with Pd [19]. The oxidative desorption of hydrogen from Pd (Eq. (1)) is considered to be the rate determining step (rds) of the HOR under alkaline conditions (Eq. (1)) [21,22].

$$Pd{-}H + OH^- \rightarrow Pd + H_2O + e^- \quad (1)$$

Hence, a weakening of the bonding of the adsorbed hydrogen can enhance significantly the kinetics. Due to the increasing complexity and challenge of the mechanism of HOR in alkaline media as compared to HOR in acidic medium, the stability of the catalyst is of concern. Due to the scarce data available on HOR catalysts in alkaline medium, stability tests of these materials have not been reported. Specifically for Pd based catalysts, while Pd dissolution in acidic media is well documented [23,24], literature data on Pd corrosion in alkaline media is very scarce. Also Pourbaix diagrams, showing stability windows for different species in the E vs. pH space, do not give any conclusive answer to whether Pd corrodes in base. According to a previous report, Pd should be extremely stable in typically used alkaline electrolytes [25]. In that report, the authors could not detect any signs of Pd dissolution in 0.5 M KOH at 25 °C. However, at alkali concentrations of 6 M KOH or higher, and at elevated temperatures some dissolution was detected. Bolzan, interpreting the results obtained using rotating ring disk electrode tests, suggested that some Pd dissolution exists in 1 M NaOH, but stressed that the dissolution rates/amounts are significantly lower than that measured in acidic electrolytes [26]. More recently, however, using identical-location transmission electron microscopy (ILTEM) coupled to electrochemistry, Zadick et al. demonstrated that the relative stability of Pd towards electrochemical dissolution in base was not a warranty for the stability of state-of-the-art carbon supported Pd nanoparticles at high pH. Indeed, the particles suffer dramatic detachment from their carbon support, overall yielding a very large decrease of electrochemical surface area (ECSA) in a rather limited number of voltammetric cycles (typically below 1000 cycles at 100 mV s^{-1} in the range $0.1 < E < 1.23$ V *vs* RHE) in 0.1 M NaOH at 25 °C [27]. Surprisingly, Pt/C nanoparticles were demonstrated to suffer even more such degradation in base electrolytes [28].

In the present study, we report our continued investigation of the properties of the Pd/C-CeO_2 catalyst, showing its enhanced HOR activity in a hydrogen-pumping cell, confirming the ceria effect on the catalytic activity of the Pd. We also report further details on its properties by comparing different Pd ratios on the same C-CeO_2 support (6 wt%, 10 wt% and 20 wt% Pd). Finally, several stability studies of the Pd-C-CeO_2 catalyst are also reported here for the first time, using both *in situ* inductively coupled plasma mass spectrometry (ICP-MS) and identical-location transmission electron microscopy experiments, as well as using hydrogen-pumping cells.

2. Experimental

All material manipulations during materials preparation, except as stated otherwise, were routinely performed under nitrogen atmosphere using standard airless technique. Carbon black (Vulcan XC-72 pellets) was purchased from Cabot Corp., USA. All metal salts and reagents were purchased from Aldrich and used as received. All the solutions were freshly prepared with doubly distilled deionized water.

2.1. Material syntheses

2.1.1. Synthesis of Pd/C (10 wt%)

Vulcan XC-72 (6.0 g) was suspended in 250 mL of ethylene glycol and sonicated for 20 min in a 500 mL three-neck round-bottomed flask. Then a solution of 1.0 g of $PdCl_2$ in a mixture of H_2O (50 mL), ethylene glycol (50 mL) and 6 mL HCl (37%) was added dropwise under stirring in a N_2 stream. After adequate stirring, an alkaline solution of NaOH (5 g) in H_2O (10 mL) and ethylene glycol (35 mL) was introduced in the reactor which then was heated at 125 °C for 3 h again under a N_2 atmosphere. Then the mixture was cooled to room temperature. The solid product was filtered off and washed with H_2O to neutral pH. The final product was dried in vacuum oven at 40 °C. (Yield: 6.53 g).

2.1.2. Synthesis of C-CeO_2 support (50:50)

Vulcan XC-72 (4 g) was added to a solution of $Ce(NO_3)_3{\cdot}6H_2O$ (10.1 g) in H_2O (250 mL). The mixture was kept under stirring for 60 min and sonicated for 30 min. After adjusting the pH to 12 with KOH, the resulting suspension was stirred for 2 h. The product was separated by filtration and washed with H_2O until neutral pH was obtained. The product was dried at 65 °C, then subsequently heated under air in a tube furnace at 250 °C for 2 h. Cooling to room temperature was undertaken under a flow of Ar. The yield of C-CeO_2 was 7.15 g.

2.1.3. Synthesis of Pd/C-CeO_2

The synthetic procedure used was the same for each catalyst with the only difference the amount of Pd salt used to obtain the desired loading of 6 wt%Pd, 10 wt%Pd and 20 wt%Pd. As an example for the 10 wt%Pd catalyst, the synthesis was as follows: C-CeO_2 (4 g) was suspended in water (500 mL), stirred vigorously for 30 min and sonicated for 20 min. To this mixture, a solution of K_2PdCl_4 (1.38 g) in water (60 mL) was slowly added (during ca. 1 h) under vigorous stirring, followed by addition of an aqueous solution of 2.5 M KOH (8.4 mL). Next, ethanol (50 mL) was added and the resulting mixture was heated at 80 °C for 60 min. The desired product Pd/C-CeO_2 was filtered off, washed several times with distilled water to neutrality and finally dried under vacuum at 65 °C until constant weigh was reached. The yield of Pd/C-CeO_2 was 4.45 g.

2.2. Electrochemical and physical characterization

Transmission electron microscopy (TEM) was performed on a Philips CM12 microscope at an accelerating voltage of 100 kV. The microscope was equipped with an EDAX energy dispersive microanalysis system. Scanning Electron Microscopy (SEM) was performed on a HITACHI S4800 microscope operating at 15 kV. High resolution TEM (HR-TEM) images were recorded with a Zeiss Libra 200 FE TEM equipped with a double tilt goniometer at 200 kV and FEI Tecnai-F30 microscope which was operated at 300 kV. The active metal surface area was determined by CO chemisorption method, adapted to carbon supported materials, at 70 °C by the use of an ASAP 2020 C Instrument (Micromeritics Corp.). Before the measurements, the samples were reduced at 210 °C with H_2 and treated in vacuum at the same temperature for 15 h.

Cyclic Voltammetry (CV) measurements were performed with a Princeton 2273 A potentiostat/galvanostat, using a three-electrode arrangement with an Ag/AgCl reference electrode and a platinum foil (25 mm×25 mm×0.1 mm) as counter electrode. No IR drop compensation was applied to any of the performed experiments. The potential scale of the CV curves was then converted to the reversible hydrogen electrode (RHE) scale.

Procedures for cell preparation for fuel cell tests are described elsewhere [19]. Membrane electrode assemblies (MEAs) (5 cm^2 active area) consisting of Ag alloy-based cathodes and Pd/C-CeO_2 based anodes with 6 wt%Pd, 10 wt%Pd, and 20 wt%Pd that were activated by operating at 50 mV in clean air (~10 ppm CO_2) (1sLPM, 1 barg, dew point 73 °C) and dry hydrogen (0.2sLPM, 3 barg, room temperature), while heating the cell from room temperature to 73 °C. Following temperature and current density stabilization, polarization curves were measured from 50 mV to open-circuit at a constant scanning rate of 0.1 V min^{-1}.

Hydrogen pump experiments were carried out using 5 cm^2 electrodes. For the purposes of these tests, three different materials were

evaluated as Hydrogen Oxidation Reaction (HOR) catalysts. Commercial Pt/C (46 wt%, 3 mg_{Pt}/cm^2 +20% ionomer layer) was used as a standard, while 10 wt% Pd/C (0.33 mg_{Pd}/cm^2 +27% ionomer layer) and 10 wt%Pd/C-CeO_2 (0.38 mg_{Pd}/cm^2 +30% ionomer layer) were also evaluated. In all cases, Pt/C electrodes identical to the standard were used as CE/RE electrodes for the Hydrogen Evolution Reaction (HER). Electrodes were prepared by spraying an ink solution composed of water, IPA, catalyst, and Nafion onto bare carbon paper supports. An additional topcoat of ionomer was also sprayed onto the electrodes. Prior to use, anion exchange membranes were hydrated for 2 h in 65 °C water, followed by a room temperature solution of 0.5 M NaOH for 1 h to complete the exchange process. The MEAs was hot-pressed for 4 min under a 3600 lb load (100 psi) at 60 °C.

Testing was done on in-house built test stations, with a cell operating temperature of 60 °C with 100% relative humidity. During cell heating and humidification, N_2 was flowed over both electrodes at 100sccm. Anode flow was then switched to H_2 at 100sccm, while the cathode flow remained unchanged.

Stabilization of the MEA was achieved by slowly ramping from 10 to 100 mA cm^{-2} (10 mA cm^{-2} increments, 1 min per step), followed by a 30 min hold at 100 mA cm^{-2}. Polarization curves were taken from 50 to at least 300 mA cm^{-2} in 50 mA cm^{-2} increments, followed by a 1 h hold at 300 mA cm^{-2}. All measurements were taken on a Metrohm Autolab (PGSTAT302N) paired with a 20 A current booster (PGSTAT30). Electrochemical Impedance Spectra (EIS) were taken potentiostatically at the potentials corresponding to the polarization curve current densities.

A modified scanning flow cell (SFC) with a 2 mm in diameter opening connected to an inductively coupled plasma mass spectrometer (ICP-MS, NexION, 300X, Perkin Elmer) was used to perform a first set of electrochemical stability tests [29]. The Pd^{106} signal was recorded in relation to the Rh^{103} as an internal standard, which was added downstream of the SFC. The flowrate was 180 μL min^{-1}. All measurements were done in a 0.05 M NaOH electrolyte. A glassy carbon plate was employed as the working electrode to support Pd/C-CeO_2 (10 wt%Pd) and Pd/C (10 wt%Pd) catalysts, while a graphite rod and an Ag/AgCl electrode were used as the counter and reference electrodes, respectively. All potentials are reported against the RHE. For preparation of the catalyst ink 8.5 mg of Pd/C-CeO_2 or Pd/C was suspended in 5 mL ultrapure water with addition of 20 μL Nafion-solution (5 wt%, Sigma-Aldrich). After ultrasonic treatment 0.3 μL of the suspension were drop-casted on the glassy carbon plate, which after drying, led to the formation of circular spots of ca. 1 mm in diameter. The resulting catalyst loading was of 6.5 μg_{Pd} cm^{-2}. Afterwards, the carbon plate containing catalyst spots was fixed under the SFC. The catalyst spots were located with the help of a vertical camera attached to the SFC. During measurements the SFC was always placed in such a way that the geometrical center of the cell and catalyst spot coincided.

Additional stability tests were performed by applying a sequence of CVs in supporting electrolyte at room temperature. The stability procedures used in this study are essentially similar to those used in the literature [27,28] to monitor the degradation of Pd/C nanoparticles (deposited on the same Vulcan XC72 carbon substrate than here and with a similar loading in Pd. A catalyst ink was prepared by mixing 10 mg of Pd/C-CeO_2 catalyst powder, 6.74 mL of ultrapure water (18.2 MΩ cm, < 3 ppb TOC, Elix + Milli-Q Gradient, Millipore), 18.8 μL of Nafion® solution (5 wt% in water and light alcohols, Electrochem. Inc.®) and 33.9 μL of isopropanol. From this ink, 20 μL was deposited at a 5 mm-diameter glassy carbon tip, yielding a surface Pd loading of *ca.* 13 μg_{Pd} cm^{-2}.

The electrochemical experiments were performed in a classical three-electrode cell connected to a VSP numeric potentiostat (Bio-Logic®). The electrolyte was an Ar-purged aqueous solution of 0.1 M NaOH at room temperature (T=25 °C); this supporting electrolyte was prepared using high-purity reagents (Merck, Suprapur®) and ultrapure water. The counter-electrode was a carbon plate to avoid pollution issues by metal cations. Hg/HgO was used as reference electrode in the same electrolyte, the potential of which was verified by comparison with a freshly-prepared RHE. All the potential values are nevertheless expressed on the RHE scale. The accelerated stress tests (AST) consisted of 150 and then 1000 CV cycles in the supporting electrolyte, within a potential range of $0.1 < E < 1.23$ V *vs.* RHE; the potential sweep rate was 100 mV s^{-1}. During this AST, CV cycles were periodically monitored. The morphology of the Pd/C-CeO_2 nanoparticles was also characterized by identical-location transmission electron microscopy (ILTEM) after 150 and 1000 CV cycles. In that case, the above-mentioned AST was reproduced using a gold + lacey carbon TEM grids as the working electrode. In ILTEM, similar regions of the catalyst are observed before/after the degradation test. The TEM used for these specific characterizations is a JEOL 2010 TEM apparatus, equipped with a LaB6 filament operating at 200 kV (point to point resolution 0.19 Å) and with an Oxford Inca® X-Ray dispersive spectrometer for local chemical analyses.

3. Results and discussion

3.1. Material characterization

The XRD diffraction patterns of the as prepared catalyst materials are shown in Fig. 1. Trace 1(a) represents the mixed carbon-ceria support and all visible peaks can be assigned to ceria-based reflections. The addition of Pd to the support can be seen by the appearance of a peak at around 40° that can be assigned to Pd metal. The small intensity and broad nature of the peak for these samples is representative of the presence of a large proportion of amorphous Pd oxides in each catalyst as has been confirmed by XAS studies in our previous report [19]. This is particularly obvious when comparing the intensity with that representative of the Pd/C sample (10 wt% Pd) in trace (e) where most of the Pd present is metallic. In-situ XRD studies have shown that the Pd oxide in the C-CeO_2 supported samples is reduced metal in the presence of flowing hydrogen [19].

The specific surface area (S_{BET} m^2 g^{-1}) of these materials was determined using Brunauer–Emmett–Teller (BET) analysis (Table 1). The value obtained for the as-obtained Vulcan XC-72R (222 m^2 g^{-1}) is in the range of what reported in the literature [30]. The addition of ceria which has a BET surface area of approximately 60 m^2 g^{-1} [31] to Vulcan XC-72 carbon with a 50:50 weight ratio reduces the surface area of the resulting mixed support C-CeO_2 (140 m^2 g^{-1}). Addition of 6 or 10 wt% Pd to C-CeO_2 does not affect significantly the values of specific surface area measured. With 20 wt% Pd, the BET surface area drops from around 140–124 m^2 g^{-1}. Table 1 also shows the active metal (Pd) surface area determined by CO chemisorption experiments. The data reported includes the Pd specific surface area m^2 $g^{-1}{}_{Pd}$ and the average crystallite size calculated from this data (nm). The 10 wt% Pd sample shows the highest Pd specific surface area (236 m^2 $g_{Pd}{}^{-1}$) and smallest calculated crystallite size (2.1 nm).

To study the catalyst morphology and surface structure, we have found that high resolution Z-contrast STEM is a good technique to elucidate the structure of these catalysts and the Pd metal distribution. In Fig. 2, images at different magnifications are shown for the Pd/C-CeO_2 materials with different Pd loadings (6 wt%, 10 wt% and 20 wt% of Pd). Firstly, it can be seen that the CeO_2 particles do not cover uniformly the Vulcan XC-72 carbon material. Some distinct agglomerated CeO_2 structures (brighter structures) can be seen separated from the Vulcan carbon. Pd nanoparticles (NPs) are visible on the bare carbon areas. It is not possible however to individualize Pd NPs on the ceria portions due to poor resolution between these two species. The number of Pd NPs visible on the carbon substrate increases along with the loading. Interestingly, few Pd particles are visible on the 6 wt% Pd sample (pointed out by arrows). More are visible on the carbon as the metal loading increases and this allows us to determine the average Pd particle size distribution (mean values determined are 2.0 nm and

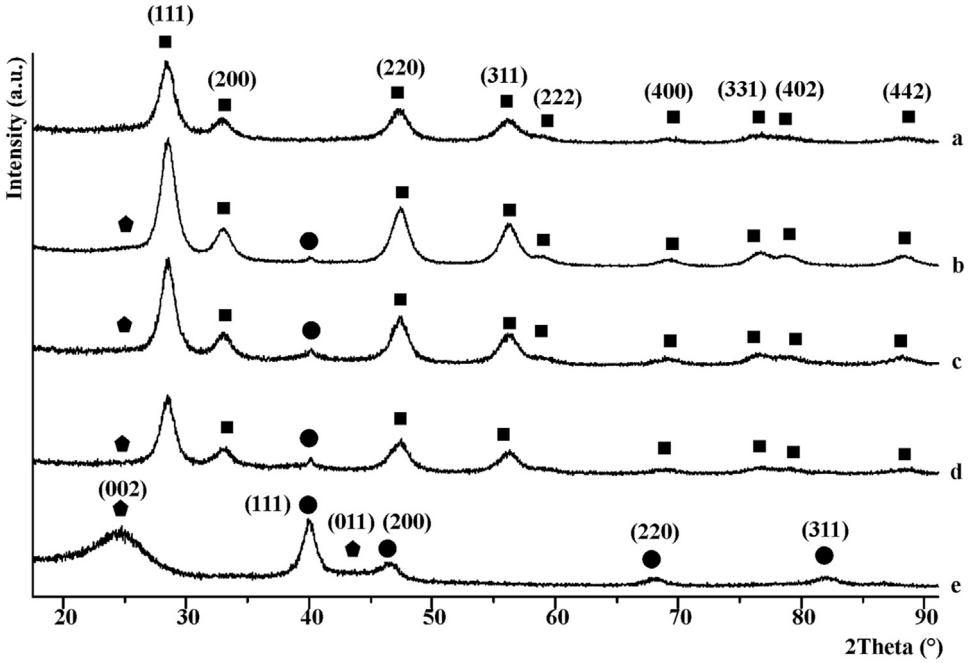

Fig. 1. XRD diffraction patterns of (a) 50:50 wt% C-CeO_2, (b) Pd/C-CeO_2 (6 wt% Pd), (c) Pd/C-CeO_2 (10 wt% Pd), (d) Pd/C-CeO_2 (20 wt% Pd) and (e) Pd/C (10 wt% Pd). Legend: (•) Pd, (■) CeO_2 and (⬟) carbon.

Table 1
Physical characterization data obtained from BET experiments and CO-chemisorption isotherms.

Sample	S_{BET} $m^2\,g^{-1}$	Pd specific surface area $m^2\,g_{Pd}^{-1}$	Pd particle size nm
C (Vulcan XC-72)	222	–	–
C-CeO_2 (50 wt% CeO_2)	140	–	–
Pd/C-CeO_2 (6 wt% Pd)	141	188	2.6
Pd/C-CeO_2 (10 wt% Pd)	145	236	2.1
Pd/C-CeO_2 (20 wt% Pd)	124	146	3.4

2.5 nm for the 10 wt% and 20 wt% samples, respectively).

STEM-EDX analysis helps to determine the Pd distribution over the whole sample including also the ceria portions of the support. As example, a representative image of the 20 wt% Pd sample is shown in Fig. 3. Two zones are clearly distinguishable. On the right side a purely carbon portion (in blue) covered with many small Pd NPs (in green). STEM-EDX elemental map analysis shows a large ceria cluster (in red) covering the carbon structure on the left portion of the sample. The Pd mapping shows that although there are many Pd NPs visible on the carbon section, most of the Pd is actually present on the ceria structures. STEM-EDX analysis of the sample prepared with 10 wt% Pd shows the same trend with the only difference being that very few Pd nanoparticles are visible on the bare carbon regions (see SI for comparative analysis). The middle set of TEM images in Fig. 2 also show clearly that there are few Pd nanoparticles visible on the carbon regions for 6 and 10 wt% Pd samples while at 20% loading there is higher coverage of Pd also on the carbon.

3.2. Electrochemical tests

Electrochemical data are listed in Table 2, including the electrochemically active surface area (ECSA), exchange current densities (i^0) and the mass activity per gram of Pd (i^0, m). The mass activity per gram of Pd is significantly higher for the 10 wt% Pd sample relative to both the 6 wt% and 20 wt% samples. The Tafel analysis of each catalyst, shown in Fig. 4, also confirms the increased performance of the 10 wt % Pd sample relative to the others. Indeed, increasing the Pd loading from 10% to 20% does not improve the overall activity of the catalyst. Tafel slope analysis reveals a large difference amongst the various catalysts with values of 100, 66 and 143 mV dec^{-1} respectively suggesting a change in the HOR mechanism after a doubling of the Pd loading 10–20%). A value of 66 mV dec^{-1} indicates that the rate determining step (rds) for the 10% Pd catalyst is molecular hydrogen dissociative adsorption (Tafel step), while the 20% Pd sample shows a value that suggests charge transfer processes are rate limiting [22].

3.3. Fuel cell tests

For fuel cell tests, the Pd/C-CeO_2 anode catalysts with different Pd loadings (6 wt%, 10 wt% and 20 wt% Pd) were incorporated into anode catalyst layers (0.15–0.30 $mg_{Pd}\,cm^{-2}$). Three identical cells where the only change was the anode catalyst layer, were prepared for testing in AEM-FC single cells. Fig. 5 shows the cell performance at 73 °C run with dry H_2 and purified air (~10 ppm CO_2). Polarization curves of cells with anodes made with Pd/C-CeO_2 (6 and 20 wt% Pd) were compared with the previous reported results made with anodes made with Pd/C-CeO_2 10 wt% Pd [19]. As can be seen from Fig. 5, although results obtained with all catalysts appear to be similar, the Pd/C-CeO_2 10 wt% Pd reported previously shows slightly better performance [19]. Table 3 summarizes the fuel cell results.

As shown in Table 3, the performance of the Pd/C-CeO_2 10 wt% Pd catalyst performs slightly better than the other two catalysts with higher and lower Pd loadings. It seems that the high Pd loading (20 wt %) does not give any beneficial effect on fuel cell performance, as increasing the amount of Pd from 10 wt% to 20 wt% leads to more Pd deposited on the carbon regions, as discussed previously and also shown in Figs. 2 and 3. These isolated Pd on carbon nanoparticles do not contribute to the enhanced activity as they perform as Pd/C, with significantly lower performance due to the lack of the advantage of Pd-ceria interactions [19].

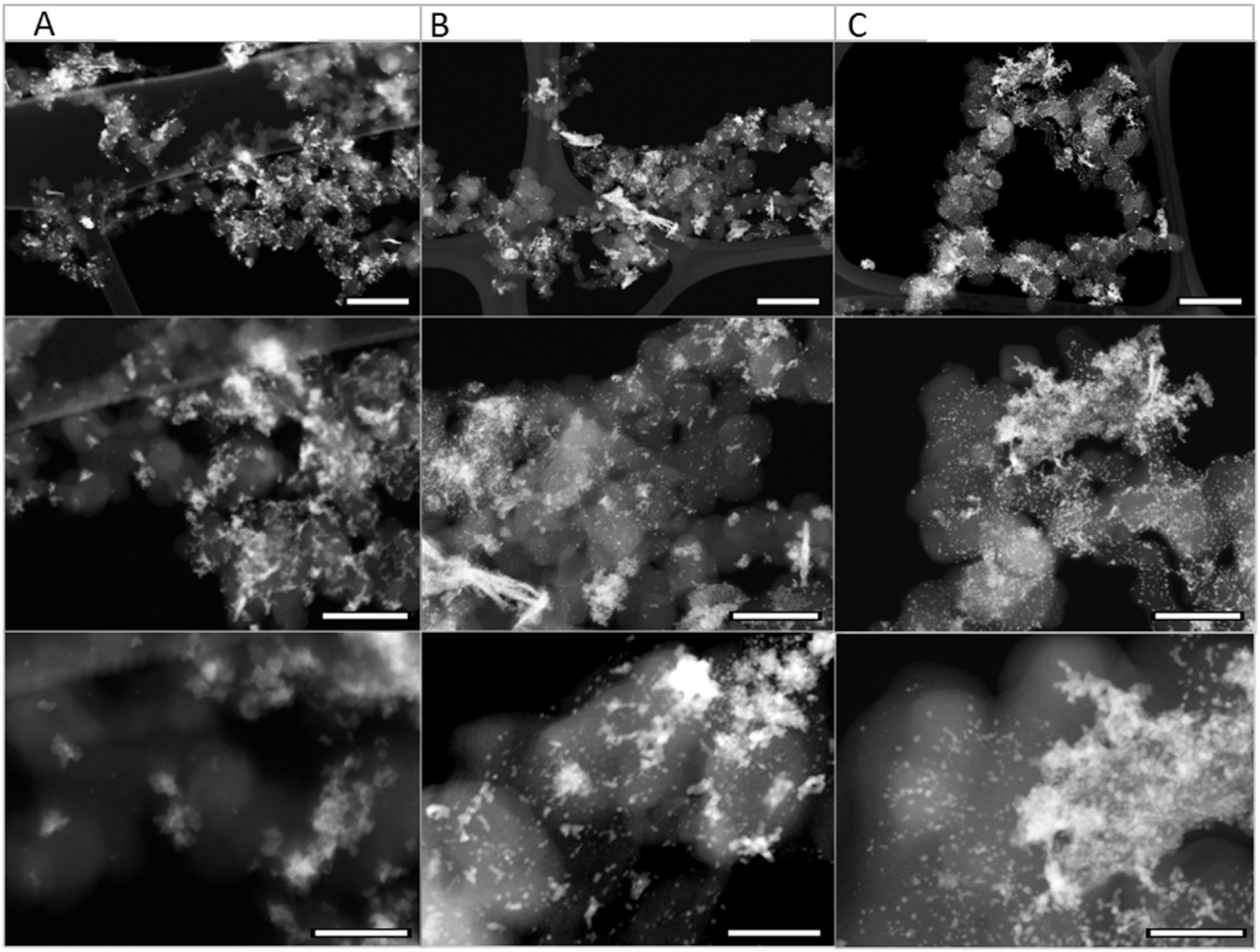

Fig. 2. Comparison between the three Pd loadings (A 6%, B 10% and C 20%) at three different magnifications: scale bar of the first line is 200 nm, middle line 100 nm and bottom line 50 nm.

3.4. Hydrogen pumping tests

A hydrogen pump cell system was developed to test the best performing catalyst Pd/C-CeO_2 (10 wt%) and compare it to Pd/C (10 wt%) and Pt/C (46 wt%). This system allows us to study the HOR activity of each catalyst under fuel cell type conditions. Fig. 6 shows the polarization curves for the three materials, demonstrating that the Pd/C-CeO_2 material far outperforms the Pd/C catalyst, while showing similar performance to that of a Pt/C anode. This is achieved with a Pd metal loading ~10 times lower than the Pt metal loading (0.33 mg_{Pd} cm^{-2} vs. 3 mg_{Pt} cm^{-2}).

As can be seen, the performance of the Pd/C-CeO_2 catalyst is clearly superior to that obtained with Pd/C. For instance, at 0.4 V and 0.8 V the current densities obtained with Pd/C-CeO_2 were around three times higher than the current densities obtained with Pd/C. These results confirm the higher activity of Pd/C-CeO_2 as compared to Pd/C (without ceria) as has also been shown in fuel cell tests [19].

Fig. 7 shows the steady state performance of a hydrogen pumping cell run at constant 300 mA cm^{-2} over the course of 1 h. While the Pd/C shows an increase in potential during test, Pd/C-CeO_2 (as well as Pt/C) shows a very stable performance at a much lower potential. These results indicate that the addition of ceria support to the catalyst improves not just the performance, but also the stability of the catalyst.

Electrochemical Impedance Spectroscopy (EIS) spectra were taken for all three HOR catalysts. Fig. 8 summarizes these results for J =300 mA cm^{-2}. All three materials showed negative shifts in the high-frequency resistance (HFR) as the current density increased. The shift in the Pt/C HFR was significantly larger (~25 mΩ) that either the Pd/C (~5 mΩ) or the Pd/C-CeO_2 (~15 mΩ). The charge transfer resistance (approximated by the distance between to the two y-intercepts) of the Pt/C was less than that of either of the two Pd-based materials. However, the Pd/C-CeO_2 did show an improvement over the Pd/C catalyst. Additionally, the HFR of the Pd/C-CeO_2 catalyst was very similar to that of the Pt/C reference.

3.5. Stability tests

To further evaluate the stability of Pd/C-CeO_2, electrochemical tests were performed using a modified SFC to measure the dissolution properties of the 10 wt% Pd/C-CeO_2 catalyst in alkaline medium compared to Pd/C. To get a first insight on the stability of the studied catalysts in alkaline media, CVs in a broad potential window (−0.05 to 1.4 V_{RHE}) of Pd oxide formation and reduction as well as hydrogen sorption and desorption were recorded in Ar-saturated 0.05 M NaOH electrolyte. The results are summarized in Fig. 9.

In Fig. 9 the upper pane shows variation of potential with time. This contains a short stay at the open circuit potential (OCV), fast cleaning cycles, two cycles recorded at 50 mV s^{-1}, short potentiostating at $-0.05V_{RHE}$, and a slow scan at 5 mV s^{-1}. The latter is added for a clear separation between anodic and cathodic dissolution processes, well known for corrosion of other noble metals in acid and base [32]. Dissolution is shown in the lower pane in Fig. 9. By comparing the Pd/C-CeO_2 catalyst with Pd/C one can clearly see that the OCV is slightly lower, while more Pd is detected in this region for Pd/C-CeO_2. This can be an indication of the cathodic dissolution of an unstable Pd oxide, which is consistent with the fact that Pd oxide is found in the Pd/C-

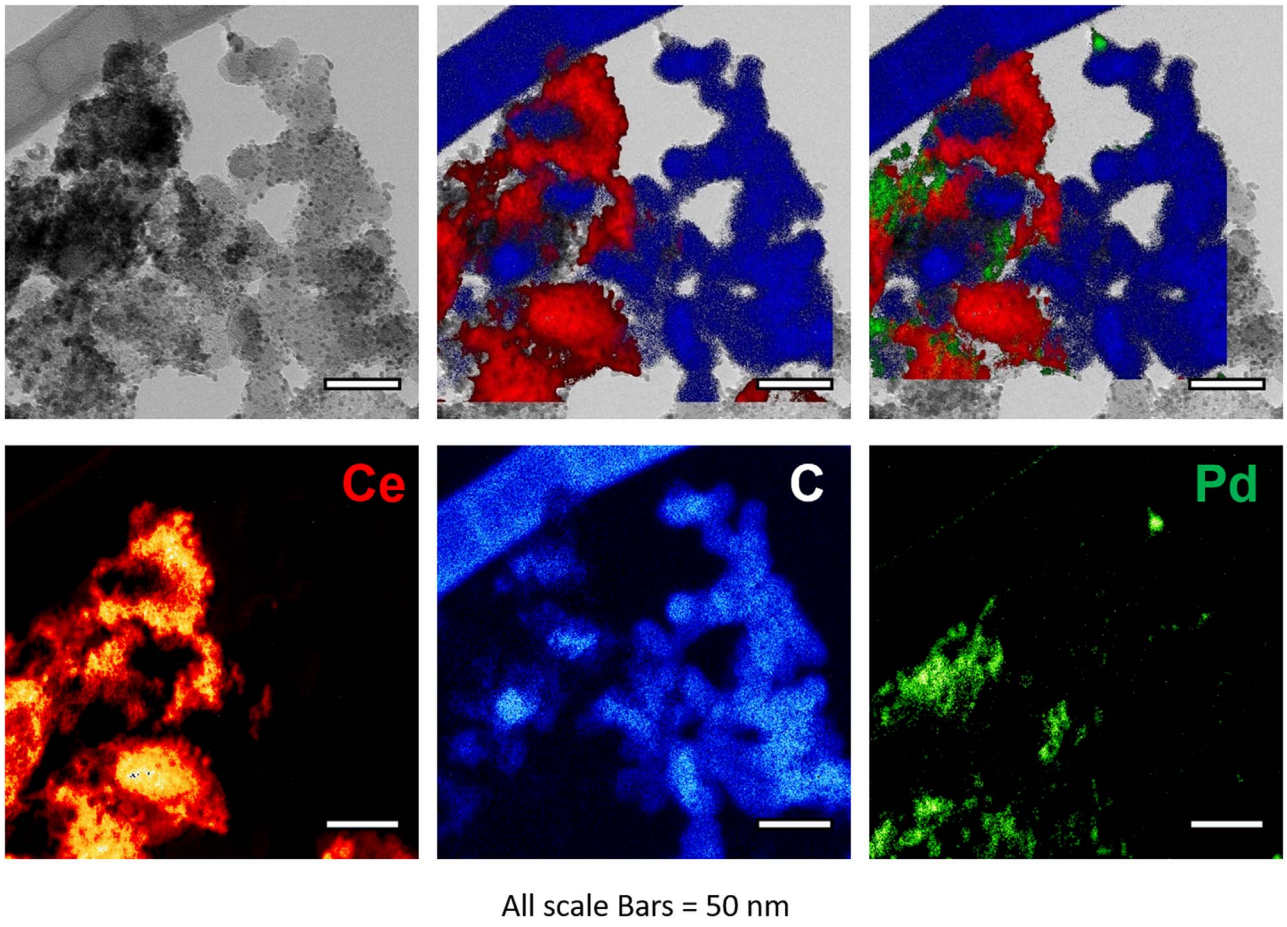

Fig. 3. STEM-EDX analysis of a representative portion of the 20 wt% Pd catalyst. (For interpretation of the references to color in this figure, the reader is referred to the web version of this article.)

Table 2
Electrochemical characterization data.

Pd content in Pd/C-CeO_2 wt%	i_0 $\mu A\ cm_{Pd}^{-2}$	ECSA $m^2\ g_{Pd}^{-1}$	Tafel slope $mV\ dec^{-1}$	$i_{0,\ m}$ $A\ g_{Pd}^{-2}$
6	89	22	100	19
10	55	43	66	24
20	83	14	143	11

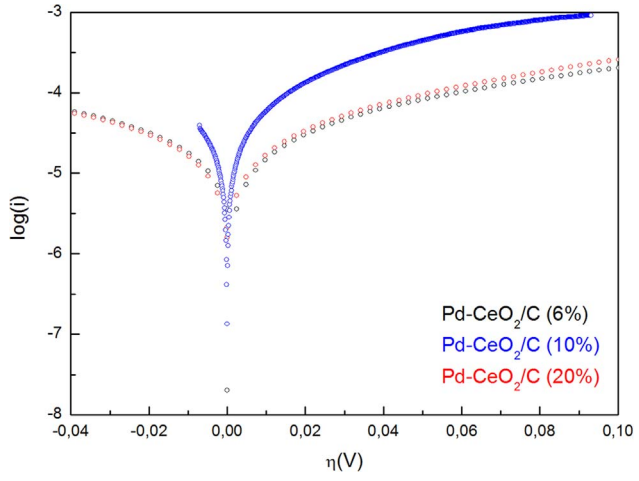

Fig. 4. Tafel slope analysis of Pd/C-CeO_2 (6 wt%, 10 wt% and 20 wt% Pd) obtained in H_2-saturated 0.1 M KOH at 10 mV s^{-1} and 1600 rpm.

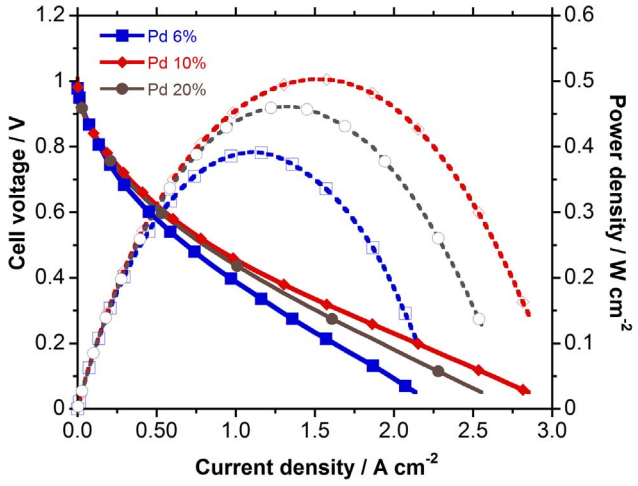

Fig. 5. Polarization curves of AEM-FCs using Pd/C-CeO_2 anode catalysts with 10 wt% Pd [19], 6%Pd and 20 wt%.

Table 3
H_2/air AEM-FC polarization data summary.

	Current density at 0.85 V $mA\ cm^{-2}$	Peak power density $mW\ cm^{-2}$
Pd/C-CeO_2 10 wt%Pd [19]	100	500
Pd/C-CeO_2 6 wt%Pd	90	390
Pd/C-CeO_2 20 wt%Pd	80	460

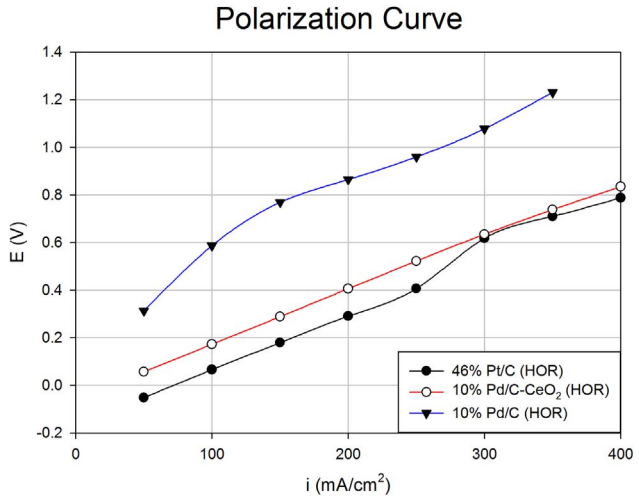

Fig. 6. Polarization curves of hydrogen pumping tests comparing the HOR performance of Pd/C-CeO_2 to both Pd/C as well as Pt/C.

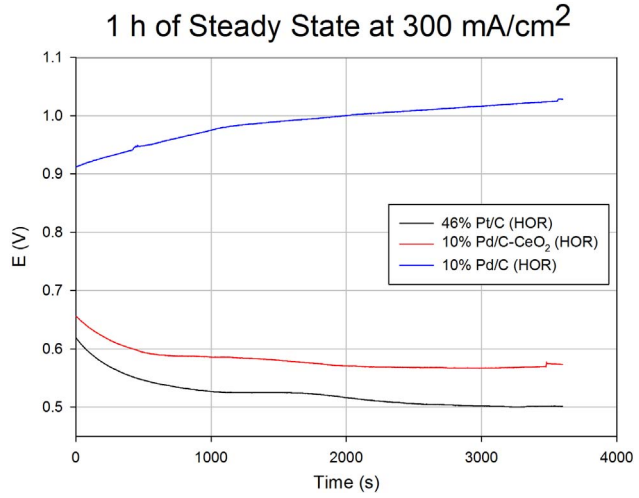

Fig. 7. Stability run of hydrogen pumping tests of Pd/C-CeO_2 catalyst as compared to both Pd/C and Pt/C under 300 mA cm^{-2} steady state operation.

CeO_2 catalyst before flowing hydrogen, which reduces the oxide layer to Pd metal (see Section 3.1). Since also some cerium dissolution was observed in this region (see Fig. S2), it can be assumed that the two

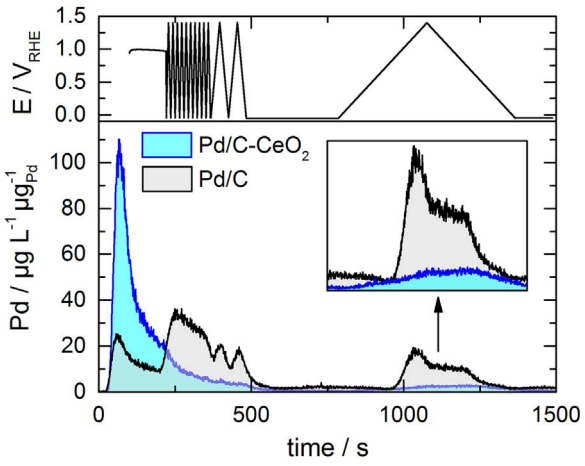

Fig. 9. Pd detection profiles of Pd/C and Pd/C-CeO_2 (both 10 wt% Pd) during 10 cycles at 200 mV s^{-1}, 2 cycles at 50 mV s^{-1} and 1 cycle at 5 mV s^{-1}, in the range of −0.05 to 1.4 V_{RHE} in 0.05 M NaOH purged with Argon.

processes are related, as it was found that Pd was preferable deposited on ceria regions (see Section 3.1). It has to be remarked though, that the observed signal must be due to dissolution but not particle detachments as in the latter case the dissolution rates of Pd and Ce should scale linearly.

From Fig. 9 it can be also seen that the Pd/C-CeO_2 catalyst stabilizes with potential cycling, although the detection of Pd by ICP-MS is still non-zero. The contrary is observed for Pd/C where Pd detection from this electrode significantly increases with potential cycling. The origin of the detection of Pd can here originate both from dissolution of the Pd nanoparticles or from their detachment from the carbon support, the latter having been found non-negligible in NaOH electrolytes by ILTEM experiments [27]. The total amount of Pd lost from both electrodes during the OCV and the potential cycling is ca. 1.4 ng, which is 3% of the initial loading. Both electrodes are stabilized during the following potential step at −0.05 V_{RHE}. When potentials move into anodic direction, Pd starts to dissolve from both electrodes. Interestingly, the onset of Pd dissolution from Pd/C-CeO_2 is significantly lower that for Pd/C (see inset in Fig. 9), suggesting a different mechanism (or different kinetics) of Pd loss. Even if initiated later, Pd/C dissolution however, shows much higher dissolution rates (up to an order of magnitude) at the higher potentials. At even higher potentials Pd passivates, likely due to formation of a stable oxide. Some increase in dissolution is also observed during oxide reduction, although the

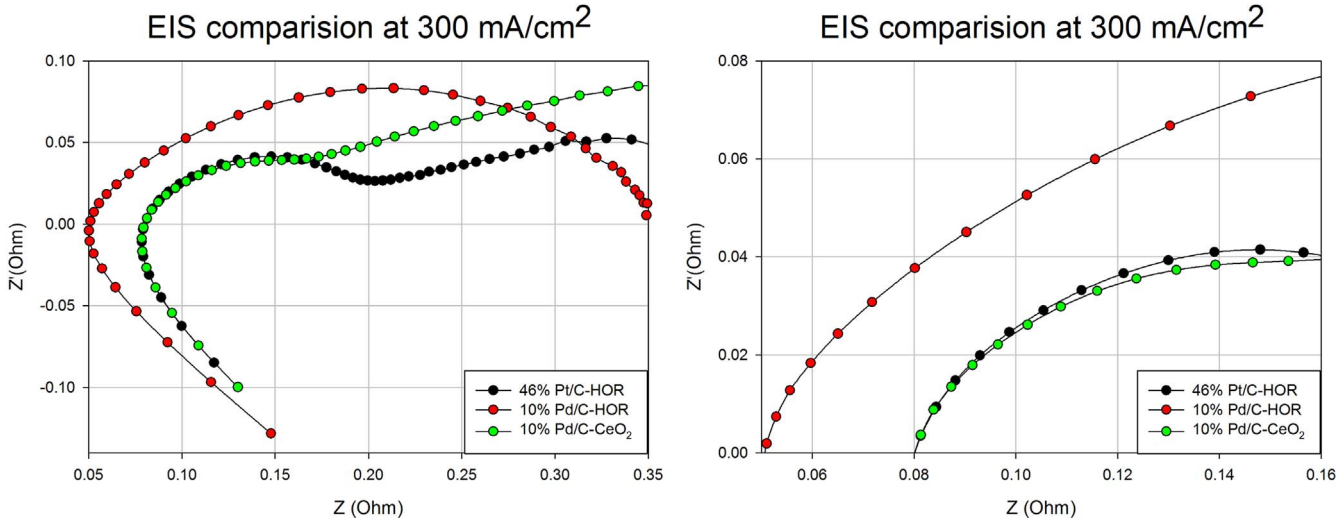

Fig. 8. EIS measured during hydrogen pumping tests at a current density of 300 mA cm^2. Right plot shows a zoom-in of the left plot.

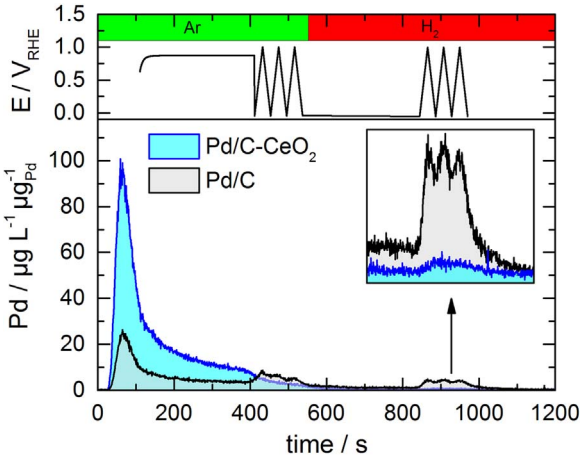

Fig. 10. Dissolution profiles of Pd/C and Pd/C-CeO_2 (10 wt%Pd) during cycling at 50 mV s^{-1} in the range of −0.05 to 1.0 V_{RHE} in 0.05 M NaOH purged with argon (in first, green left area) and then with hydrogen (in second, red right area). (For interpretation of the references to color in this figure legend, the reader is referred to the web version of this article.)

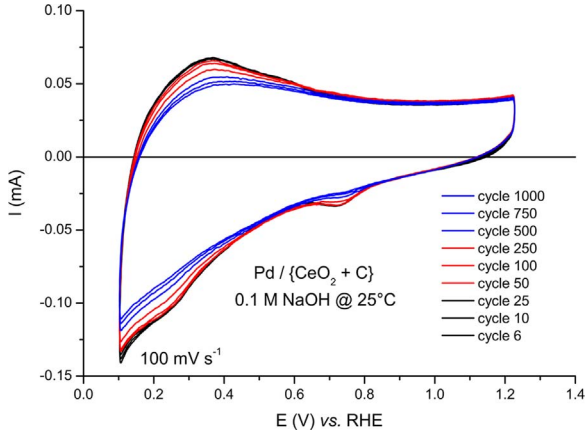

Fig. 11. CVs monitored on the Pd/C-CeO_2 (10 wt%Pd) catalyst upon aging in 0.1 M NaOH supporting electrolyte at 25 °C.

amounts are lower. As previously indicated, the reason for the superior stability of Pd/C-CeO_2 may be a strong Pd-ceria interaction. As demonstrated by STEM and XAS investigations in our recent article most of the Pd nanoparticles are supported on the CeO_2 (and not on carbon) [19], and are therefore not subjected to the harsh nanoparticle detachment that occurs for carbon-supported Pd/C nanoparticles. This hypothesis will be explored by ILTEM experiments (see below).

It is anticipated that during normal operation of an AEM-FC the highest anodic potential the anode will experience is the potential at open circuit (0.9–1.0 V vs RHE), which is significantly lower than the upper potential limit of cycling used in the experiments presented in Fig. 9 (=1.4 V vs RHE). Also, as hydrogen can influence (reduce) the Pd oxide layer of the Pd/C-CeO_2 catalyst, a second protocol shown in Fig. 10 was used to investigate Pd stability at much more realistic conditions (better simulating an AEM-FC environment). In this case, the upper potential limit was moved to 1.0 V_{RHE} and the cleaning cycles were excluded. Moreover, dissolution was studied in argon as well as in hydrogen, to test if hydrogen influences stability and to see if the improved activity of Pd/C-CeO_2 towards HOR holds also in SFC tests.

For both electrodes, the dissolution behavior during the OCV and potential cycling in argon is analogous to that discussed above. Furthermore, no significant difference was observed when the gas was switched to hydrogen. In hydrogen, Pd behaves similarly to Pt in acid [33]. The inset in Fig. 10 presents a magnified view of the dissolution profile, where it can be clearly seen that the amount of Pd dissolved from Pd/C-CeO_2 is significantly lower as compared to that dissolved from Pd/C, indicating that the stability of the Pd/C-CeO_2 is remarkable higher than the stability of Pd/C. In this region, the estimated amount of dissolved Pd was 50 pg and 5 pg for Pd/C and Pd/C-CeO_2, respectively. Hence, assuming that dissolution rate is not changing with material consumption (a very rough estimation) all Pd should be completely dissolved in 3000 and 30,000 cycles up to 1.0 V_{RHE} from the Pd/C and Pd/C-CeO_2 electrodes, respectively. These results suggest that the excellent stability of the Pd/C-CeO_2 may be related to the Pd-ceria interaction.

To further examine the stability of the Pd/C-CeO_2 catalyst and investigate the mechanisms of degradation of these materials, CV cycling tests were also performed and analyzed. Fig. 11 presents a sequence of CVs obtained on the Pd/C-CeO_2 (10 wt%Pd) catalyst upon aging in 0.1 M NaOH (at 25 °C) supporting electrolyte. It can be seen that the overall shape of the CV is very similar to that obtained on the same material in 0.1 M KOH, previously reported [19], although in that latter case, the peak related to Pd-oxides reduction was more pronounced, because the upper vertex potential was larger (1.3 V *vs.* RHE instead of 1.4 V *vs.* RHE) and the scan rate value was lower. One also clearly sees that the signature of Pd-hydrides and Pd-oxides gradually level off upon cycling.

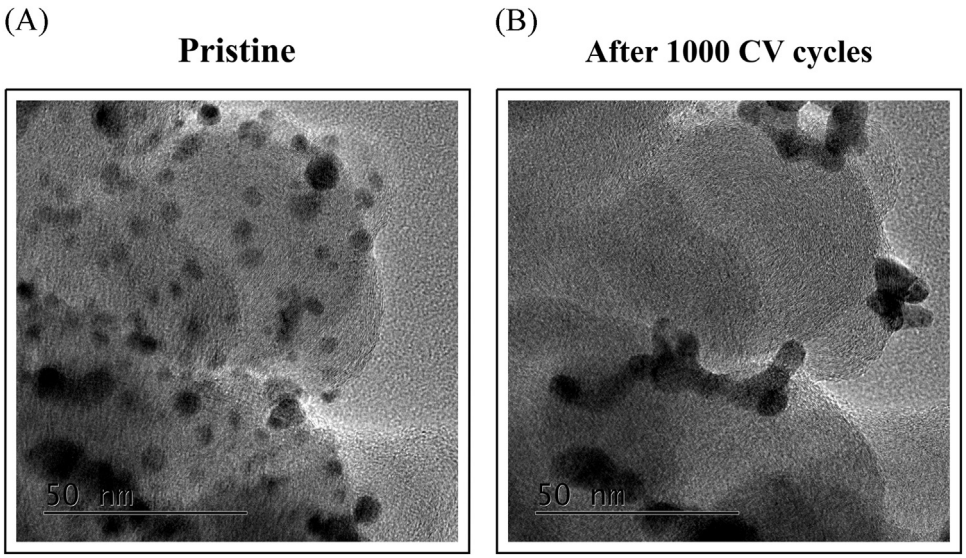

Fig. 12. Selected ILTEM micrographs of the Pd/C sample in (A) its pristine state, and (B) after 1000 CV cycles in 0.1 M NaOH at 25 °C.

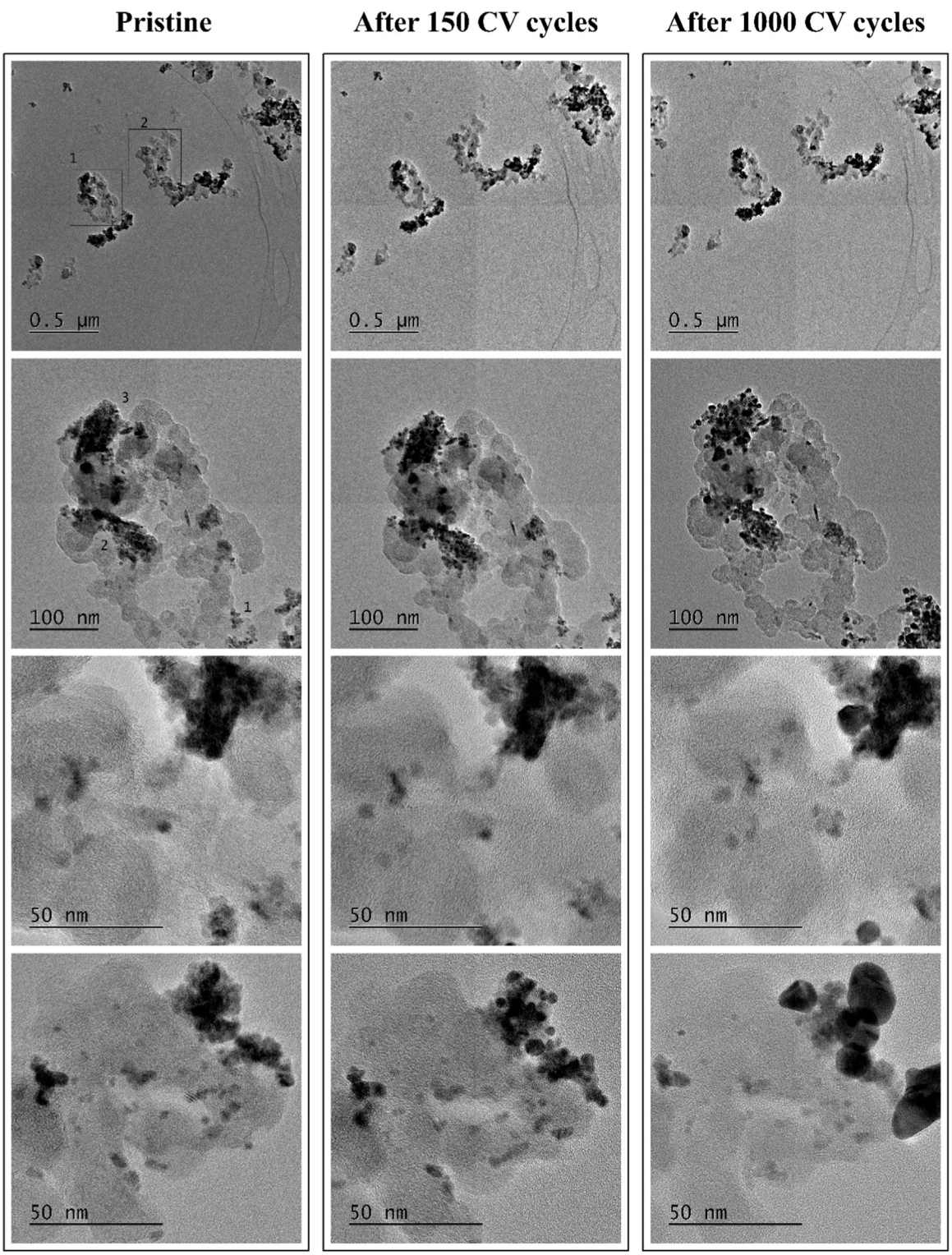

Fig. 13. ILTEM micrographs of the Pd/C-CeO_2 sample in its pristine state (left), and after 150 (center) and then 1000 CV (right) cycles in 0.1 M NaOH at 25 °C. Although the vast majority of the Pd/C-CeO_2 nanoparticles undergo extensive agglomeration/coalescence (top micrographs), some (very few) regions are subjected to much less growth of the Pd crystallites and are subjected to (minor) loss of Pd nanoparticles (bottom micrographs).

To complement the electrochemical experiments, ILTEM micrographs were acquired for Pd/C-CeO_2 after 150 and 1000 CV cycles (Fig. 13) and for comparison, ILTEM micrographs of the Pd/C sample in its pristine state, and after 1000 CV are shown in Fig. 12. For Pd/C (and this has been observed in a similar manner for "large" and "small" nanoparticles of Pd/C [27,28], more than 50% of the Pd nanoparticles were lost in the experiment, probably due to detachment of the nanoparticles from the carbon substrate (Fig. 12). Further stability tests are needed to clearly determine whether detachment of the particles actually occurs. Fig. 13 shows for the same aging test with Pd/C-CeO_2, that no major loss of Pd nanoparticles is observed, even after 1000 CV cycles.

In the case of the Pd/C-CeO_2 nanoparticles, the mechanisms at stake in the degradation test are completely different than for Pd/C.

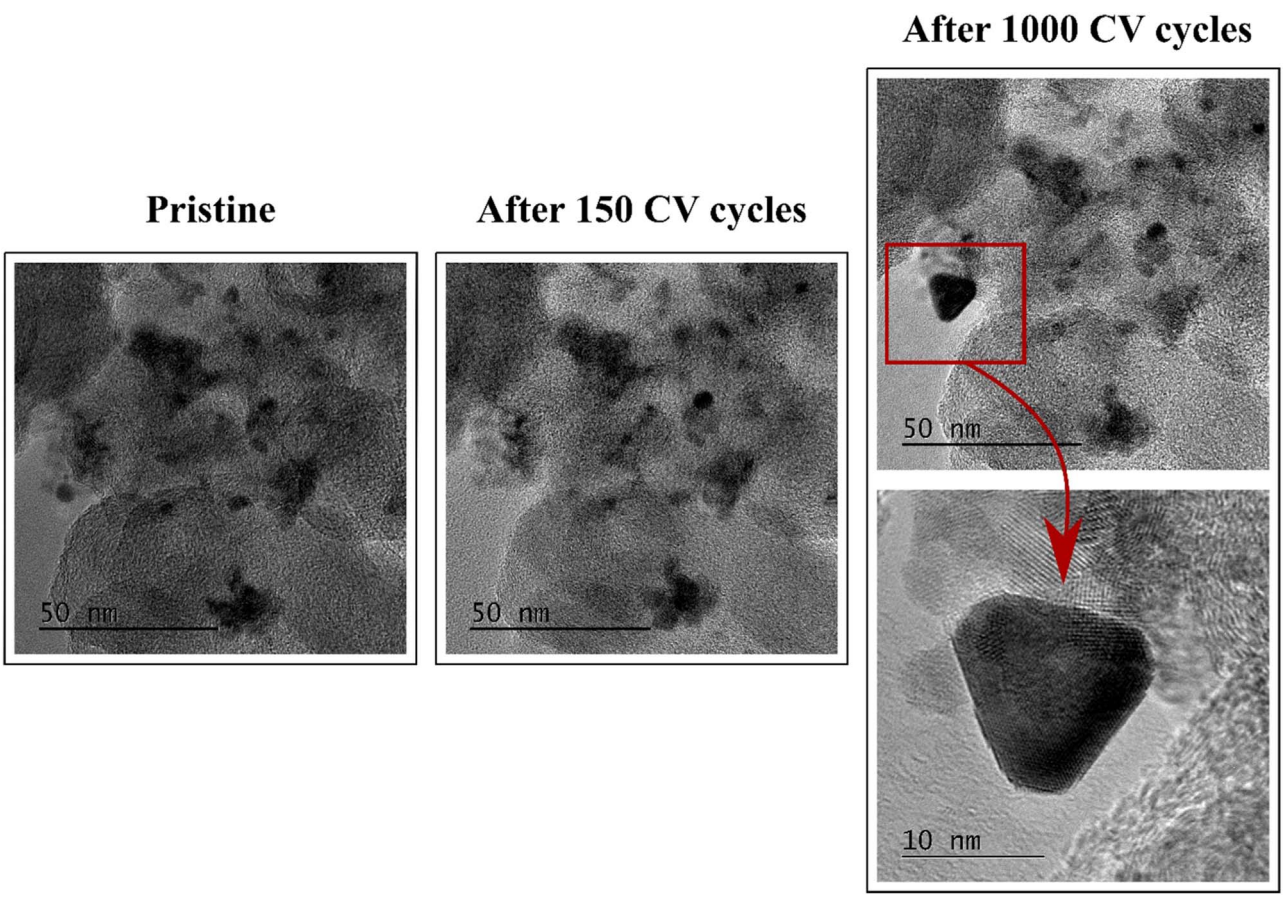

Fig. 14. High-magnification micrographs of a grown monocrystalline Pd nanoparticle in contact with several smaller CeO_2 nanoparticles, for the Pd/C-CeO_2 catalyst; pristine (left), and after 1000 cycles (middle and right).

The micrographs of Fig. 13 indeed show no consequent detachment of nanoparticles, but instead, their shape is progressively and severely modified upon cycling. Whereas the Pd crystallites of Pd/C-CeO_2 were (agglomerated but) small initially (*ca.* 2.1 nm in diameter [27]), they grow after 150 and especially 1000 CV cycles in supporting electrolyte. After 1000 CV, the originally agglomerated, small, and ill-defined Pd nanoparticles (all these observations agree with the results of XRD, CO-chemisorption and SEM/TEM presented above) are transformed into much larger and round-shape (for most of them) single crystalline nanoparticles (Fig. 13). This process is a clear coalescence of the Pd nanoparticles initially present within agglomerates, probably according to a dissolution/redisposition mechanism on a short distance scale. It is worth noting that no new nanoparticles are created by the degradation, which rules out massive random redisposition, and the change of shape of isolated (not initially agglomerated) nanoparticles is very minimal, ruling out the *usual* 3D Ostwald ripening mechanism at long scale. In addition, it seems that when the Pd nanoparticles were initially not agglomerated (isolated), they remained isolated afterwards, and that the extent of detachment is much less than observed for a Pd/C sample (see Zadick et al. [28] and Fig. 12). This is particularly obvious on the selected micrographs of Fig. 14.

In summary from ILTEM and CV aging studies, we can also say that the Pd/C-CeO_2 sample is much more stable in these operating conditions than its Pd/C counterpart. It is likely that the strong interaction of Pd with the CeO_2 and the related "more oxidized" state of Pd atoms do have a favorable impact on the durability of the Pd nanoparticles [19]. In addition, as most of the Pd nanoparticles in Pd/C-CeO_2 are in the vicinity of the CeO_2, the latter being previously coated onto the Vulcan carbon, it can be speculated that the Pd nanoparticles in Pd/C-CeO_2 are mostly not in direct contact with the surface of the Vulcan carbon, as demonstrated in the high-resolution images of Fig. 14. This hypothesis is also in agreement with the pronounced decrease of the BET area of the CeO_2-coated Vulcan versus the pure Vulcan carbon (see Section 3.1), which is compatible with the coating of the latter and related coverage/plugging of the micropores inside the carbon particles.

As it is precisely the interface of the Pd with carbon which is believed to be altered upon AST for the Pd/C samples (see Fig. 12) [27], one may understand why the Pd/C-CeO_2 sample is more robust than Pd/C in terms of particle detachment. However, this robustness is not a guaranty of complete stability, since instead of particle detachment; the agglomerates of Pd nanoparticles supported on the C-CeO_2 substrate suffer extensive coalescence into larger nanoparticles. This extensive dissolution/redisposition essentially proceeds at short distance scale (essentially inside existing agglomerates but not from groups of nanoparticles separated by several 10 nm or more), as illustrated in Fig. 13. Fig. 14 shows another remarkable example of such processes; in this case, the HRTEM images show that the grown Pd nanoparticle is clearly supported on CeO_2 crystals and not directly on the carbon substrate.

It can be pointed out that such dissolution/redisposition at short range agrees with the ICP-MS findings of Figs. 9 and 10; such a process has also already been witnessed for unsupported Pd nanocubes [34]. Two hypotheses can be put forth to account for the different mechanisms of degradation of the Pd nanoparticles in Pd/C and Pd/C-CeO_2: on the one hand, the fate of large Pd ensembles (agglomerates, more present in the initial Pd/C-CeO_2 sample than in the Pd/C ones previously [27] tested could differ from that of isolated Pd because (i) the proximity between individual crystallites in agglomerates could favor short-scale dissolution/redisposition of Pd or (ii) these large

ensembles could have more anchoring points to the substrate. On the other hand, as previously hypothesized, it can be that the stability of the Pd/C-CeO_2 nanoparticles are uniquely linked to the proximity of Pd to the CeO_2 phase (anchoring points of the Pd nanoparticles to the Vulcan carbon (see Fig. 12), which are prone to destruction in these conditions, are replaced by tougher anchoring points to the CeO_2 surface, see Fig. 14), again in agreement with the findings of ICP-MS. More studies are necessary to understand precisely the mechanisms of degradation of these materials, but this does not put into question the much enhanced durability of the Pd/C-CeO_2 nanoparticles noted here compared to Pd/C catalysts.

4. Conclusions

We report a new class of bifunctional electrocatalyst for the hydrogen oxidation reaction in fuel cells under alkaline conditions. The electrocatalysts, denoted Pd/C-CeO_2, consist of deposited Pd nanoparticles on a support mixture of 50:50 carbon and CeO_2. The Pd is preferentially deposited on the ceria regions of the support. Previous reports on AEM-FCs as well as the hydrogen pump tests described in this report show that the Pd/C-CeO_2 catalyst has significantly higher activity than Pd/C towards the HOR in alkaline medium. In addition, we have performed preliminary stability studies on Pd/C-CeO_2 showing that catalyst stability under harsh potential cycling is improved as compared to Pd/C. To the best of our understanding, the Pd/C-CeO_2 bifunctional material studied in this report is the HOR electrocatalyst with highest activity and stability for AEM-FCs so far developed.

Acknowledgements

We acknowledge the Ente Cassa di Risparmio di Firenze ITALY (projects HYDROLAB2 and EnergyLab) for financial support. This work was also partially funded by the Grand Technion Energy Program (GTEP); by the European Commission through H2020 Grant No. NMBP-03-2016 CREATE project; by the Ministry of Science, Technology & Space of Israel through the M.era-NET Transnational Call 2015, NEXTGAME project; and by the Israel National Research Center for Electrochemical Propulsion (INREP-ISF).

Appendix A. Supporting information

Supporting information associated with this article can be found in the online version at doi:10.1016/j.nanoen.2017.01.051.

References

[1] J.R. Varcoe, P. Atanassov, D.R. Dekel, A.M. Herring, M.A. Hickner, P.A. Kohl, A.R. Kucernak, W.E. Mustain, K. Nijmeijer, K. Scott, T.W. Xu, L. Zhuang, Anion-exchange membranes in electrochemical energy systems, Energy Environ. Sci. 7 (2014) 3135–3191.
[2] Y.S. Li, T.S. Zhao, A passive anion-exchange membrane direct ethanol fuel cell stack and its applications, Int J. Hydrog. Energy 41 (2016) 20336–20342.
[3] Y.S. Li, Y.L. He, An all-in-one electrode for high-performance liquid-feed micro polymer electrolyte membrane fuel cells, J. Electrochem. Soc. 163 (2016) F663–F667.
[4] Y.S. Li, J.H. Lv, Y.L. He, A monolithic carbon foam-supported Pd-based catalyst towards ethanol electro-oxidation in alkaline media, J. Electrochem. Soc. 163 (2016) F424–F427.
[5] Y.S. Li, A liquid-electrolyte-free anion-exchange membrane direct formate-peroxide fuel cell, Int J. Hydrog. Energy 41 (2016) 3600–3604.
[6] Y.S. Li, H. Wu, Y.L. He, Y. Liu, L. Jin, Performance of direct formate-peroxide fuel cells, J. Power Sources 287 (2015) 75–80.
[7] Y.S. Li, Y.L. He, W.W. Yang, A high-performance direct formate-peroxide fuel cell with palladium-gold alloy coated foam electrodes, J. Power Sources 278 (2015) 569–573.
[8] Y.S. Li, Y.L. He, Layer reduction method for fabricating Pd-coated Ni foams as high-performance ethanol electrode for anion-exchange membrane fuel cells, RSC Adv. 4 (2014) 16879–16884.
[9] J. Ponce-Gonzalez, D.K. Whelligan, L. Wang, R. Bance-Soualhi, Y. Wang, Y. Peng, H. Peng, D.C. Apperley, H.N. Sarode, T.P. Pandey, A.G. Divekar, S. Seifert, A.M. Herring, L. Zhuang, J.R. Varcoe, High performance aliphatic-heterocyclic benzyl-quaternary ammonium radiation-grafted anion-exchange membranes, Energy Environ. Sci. 9 (2016) 3724–3735.
[10] L. Wang, E. Magliocca, E.L. Cunningham, W.E. Mustain, S.D. Poynton, R. Escudero-Cid, M.M. Nasef, J. Ponce-Gonzalez, R. Bance-Souahli, R.C.T. Slade, D.K. Whelligan, J.R. Varcoe, An optimised synthesis of high performance radiation-grafted anion-exchange membranes, Green Chem. (2017). http://dx.doi.org/10.1039/c6gc02526a.
[11] E.F. Holby, P. Zelenay, Linking structure to function: the search for active sites in non-platinum group metal oxygen reduction reaction catalysts, Nano Energy 29 (2016) 54–64.
[12] O.V. Korchagin, V.A. Bogdanovskaya, M.R. Tarasevich, A.V. Kuzov, G.V. Zhutaeva, M.V. Radina, V.T. Novikov, V.V. Zharikov, Characteristics of non-platinum cathode catalysts for a hydrogen-oxygen fuel cell with proton- and anion-conducting electrolytes, Catal. Ind. 8 (2016) 265–273.
[13] K. Strickland, M.W. Elise, Q.Y. Jia, U. Tylus, N. Ramaswamy, W.T. Liang, M.T. Sougrati, F. Jaouen, S. Mukerjee, Highly active oxygen reduction non-platinum group metal electrocatalyst without direct metal-nitrogen coordination, Nat. Commun. 6 (2015).
[14] A. Amel, N. Gavish, L. Zhu, D.R. Dekel, M.A. Hickner, Y. Ein-Eli, Bicarbonate and chloride anion transport in anion exchange membranes, J. Membr. Sci. 514 (2016) 125–134.
[15] A. Amel, S.B. Smedley, D.R. Dekel, M.A. Hickner, Y. Ein-Eli, Characterization and chemical stability of anion exchange membranes cross-linked with polar electron-donating linkers, J. Electrochem Soc. 162 (2015) F1047–F1055.
[16] D.R. Dekel, Alkaline membrane fuel cell (AMFC) materials and system improvement - state-of-the-art, ECS Trans. 50 (2013) 2051–2052.
[17] J. Durst, A. Siebel, C. Simon, F. Hasche, J. Herranz, H.A. Gasteiger, New insights into the electrochemical hydrogen oxidation and evolution reaction mechanism, Energy Environ. Sci. 7 (2014) 2255–2260.
[18] M. Alesker, M. Page, M. Shviro, Y. Paska, G. Gershinsky, D.R. Dekel, D. Zitoun, Palladium/nickel bifunctional electrocatalyst for hydrogen oxidation reaction in alkaline membrane fuel cell, J. Power Sources 304 (2016) 332–339.
[19] H.A. Miller, A. Lavacchi, F. Vizza, M. Marelli, F. Di Benedetto, F.D.I. Acapito, Y. Paska, M. Page, D.R. Dekel, A Pd/C-CeO2 anode catalyst for high-performance platinum-free anion exchange membrane fuel cells, Angew. Chem. Int. Ed. 55 (2016) 6004–6007.
[20] D. Strmcnik, M. Uchimura, C. Wang, R. Subbaraman, N. Danilovic, D. van der Vliet, A.P. Paulikas, V.R. Stamenkovic, N.M. Markovic, Improving the hydrogen oxidation reaction rate by promotion of hydroxyl adsorption, Nat. Chem. 5 (2013) 300–306.
[21] Y. Wang, G.W. Wang, G.W. Li, B. Huang, J. Pan, Q. Liu, J.J. Han, L. Xiao, J.T. Lu, L. Zhuang, Pt-Ru catalyzed hydrogen oxidation in alkaline media: oxophilic effect or electronic effect?, Energy Environ. Sci. 8 (2015) 177–181.
[22] S. St John, R.W. Atkinson, R.R. Unocic, T.A. Zawodzinski, A.B. Papandrew, Ruthenium-alloy electrocatalysts with tunable hydrogen oxidation kinetics in alkaline electrolyte, J. Phys. Chem. C 119 (2015) 13481–13487.
[23] S. Cherevko, A.R. Zeradjanin, A.A. Topalov, N. Kulyk, I. Katsounaros, K.J.J. Mayrhofer, Dissolution of noble metals during oxygen evolution in acidic media, Chemcatchem 6 (2014) 2219–2223.
[24] B.R. Shrestha, A. Nishikata, T. Tsuru, Channel flow double electrode study on palladium dissolution during potential cycling in sulfuric acid solution, Electrochim. Acta 70 (2012) 42–49.
[25] J.F. Llopis, J.M. Gamboa, L. Victori, Electrochim. Acta 17 (1972) 2225–2230.
[26] A.E. Bolzan, Phenomenological aspects related to the electrochemical-behavior of smooth palladium electrodes in alkaline-solutions, J. Electroanal. Chem. 380 (1995) 127–138.
[27] A. Zadick, L. Dubau, U.B. Demirci, M. Chatenet, Effects of Pd nanoparticle size and solution reducer strength on Pd/C electrocatalyst stability in alkaline electrolyte, J. Electrochem. Soc. 163 (2016) F781–F787.
[28] A. Zadick, L. Dubau, N. Sergent, G. Berthome, M. Chatenet, Huge instability of Pt/C catalysts in alkaline medium, ACS Catal. 5 (2015) 4819–4824.
[29] S.O. Klemm, A.A. Topalov, C.A. Laska, K.J.J. Mayrhofer, Coupling of a high throughput microelectrochemical cell with online multielemental trace analysis by ICP-MS, Electrochem. Commun. 13 (2011) 1533–1535.
[30] Y. Holade, C. Morais, K. Servat, T.W. Napporn, K.B. Kokoh, Enhancing the available specific surface area of carbon supports to boost the electroactivity of nanostructured Pt catalysts, Phys. Chem. Chem. Phys. 16 (2014) 25609–25620.
[31] N. Laosiripojana, S. Assabumrungrat, The effect of specific surface area on the activity of nano-scale ceria catalysts for methanol decomposition with and without steam at SOFC operating temperatures, Chem. Eng. Sci. 61 (2006) 2540–2549.
[32] S. Cherevko, A.R. Zeradjanin, G.P. Keeley, K.J.J. Mayrhofer, A Comparative study on gold and platinum dissolution in acidic and alkaline media, J. Electrochem. Soc. 161 (2014) H822–H830.
[33] A.A. Topalov, A.R. Zeradjanin, S. Cherevko, K.J.J. Mayrhofer, The impact of dissolved reactive gases on platinum dissolution in acidic media, Electrochem. Commun. 40 (2014) 49–53.
[34] A. Zadick, L. Dubau, A. Zalineeva, C. Coutanceau, M. Chatenet, When cubic nanoparticles get spherical: an identical location transmission electron microscopy case study with Pd in alkaline media, Electrochem. Commun. 48 (2014) 1–4.

Hamish Andrew Miller is a researcher at the ICCOM institute of the CNR based in Florence, Italy. After receiving his PhD in inorganic chemistry from the Queen's University of Belfast (UK) in 1999, he spent 10 years working in the chemical industry including 6 years developing fuel cells and electrolyzers. His major research interests involve nanotechnology and electrocatalysis in energy related fields. In particular developing non PGM electrocatalysts for alkaline anion exchange membrane fuel cells, electroreforming of renewable alcohols for co-production of chemicals and hydrogen and investigating the electrochemical reduction of CO_2 to fuels and chemicals.

Dr. Francesco Vizza is Research Director at the ICCOM-CNR, Florence, Italy and the scientific director of a laboratory of advanced materials for energy (LAME@ ICCOM). At the LME@ICCOM research activities, include the synthesis of catalysts for fuel cells (DAFC and PEMFC), evolution of hydrogen by electrolysis from renewables, CO_2 conversion in fuels or chemicals, development of photocatalysts for H_2 evolution, catalysts for hydrogen evolution by controlled hydrolysis or thermolysis of metal hydrides, recovery of metals from waste lithium batteries. He is author of 170 peer-reviewed publications in qualified international journals, 33 patents, 2 monographs and 8 chapters in specialized books.

Marcello Marelli received his master degree in Analytical Chemistry in 2005 and his PhD in Chemical Science in 2008 from the University of Insubria (Como, Italy). From 2009 worked at ISTM-CNR in Milan as post-doc researcher in the heterogeneous catalysis group for energy applications and chemical industry. From 2017 is a research scientist in the same group. His work is focused on the advanced morphological and chemical structure characterization of nanostructured materials for catalysis, photocatalysis and electrocatalysis via electron microscopy TEM and SEM.

Anicet ZADICK received in 2016 his PhD in electrocatalysis from Grenoble-Alpes University (France) under the supervision of Marian CHATENET and Christophe GEANTET. His PhD research focused on hydrogen storage alternatives and non-precious electrocatalysts for the direct electrooxidation of hydrazine borane in alkaline media. He is now working as energy storage specialist in the private sector.

Laetitia Dubau received her PhD on Electrocatalysis from Poitiers University (France) under the supervision of Claude Lamy and Jean-Michel Léger. After five years of post-doctoral researches on durability of PEMFC electrocatalysts in the Interfacial Electrochemistry group of Grenoble University (France), she became a CNRS researcher in 2014 in the same team. Her research interests focus on understanding the activity/stability relationships in electrocatalysis and on the design of electrocatalysts with low precious metal content.

Marian Chatenet graduated as an engineer in materials sciences and a master in electrochemistry in 1997 from the Grenoble Institute of Technology (Grenoble-INP). He defended his PhD in Electrochemistry in 2000 (Grenoble-INP) and then moved to the University of Minnesota until 2002 as a post-doctoral fellow in chemical engineering. He was appointed associate professor in Grenoble-INP in 2002, as a teacher in electrochemistry and a researcher in electrocatalysis, and is now professor in the same institute. His research topics deal with electrocatalysis of complex reactions and activity/durability of electrocatalysts, in particular for fuel cell applications.

Simon Geiger studied chemistry at the University of Stuttgart and received his MSc in 2014. Since then he is PhD candidate in the electrocatalysis group of Dr. Karl J.J. Mayrhofer at the Max-Planck-Institut für Eisenforschung. His research activities focus on electrochemical stability of iridium based materials for the oxygen evolution reaction.

Serhiy Cherevko received his PhD from the Sungkyunkwan University in 2009, where he remained until 2011. He then spent four years with Prof. K.J.J. Mayrhofer at the Max-Planck-Institut für Eisenforschung before becoming a team leader at Forschungszentrum Jülich. His research interests focus on stability of electrocatalyst materials, fundamental understanding of the electrocatalyst degradation mechanisms, and development of new experimental techniques for electrocatalysis.

Huong Doan graduated on May 2014 from Worcester State University, Worcester, MA. She is in her third year of pursuing her Ph.D at Mukerjee's lab (NUCRET, Boston, MA). Her previous publication focused on a non-PGM OER catalyst, Ni-Fe (Co)/ Raney-PANI, which was published on November 2015. She also has experience on developing and optimizing the water splitting cell system, with the main purpose of producing hydrogen gas at low cost in alkaline media, using non-PGM OER and HER catalysts (both were developed at NUCRET). Two of her current projects are funded by the DoE and partnered with Proton On-Site (Connecticut) and Pajarito (New Mexico).

Ryan K. Pavlicek got his Bachelors of Science from Carnegie Mellon University in 2011, and has since been a PhD Candidate at Northeastern University in Boston, MA, working under the direction of Prof. Sanjeev Mukerjee as well as the Northeastern University Center for Renewable Energy Technology (NUCRET). His primary research focus has been the use of non-precious metal catalysts in fuel cells, primarily funded through the Department of Energy. His work has involved the study of catalysts for both the Hydrogen Oxidation Reaction (HOR) and the Oxygen Reduction Reaction (ORR) in PEMFCs, HT-PEMFCs, and AEMFCs, focusing on performance, stability, and the investigation of mass transport effects.

Dr. Sanjeev Mukerjee is a Distinguished Professor of Chemistry and Chemical Biology at Northeastern University in Boston, MA. The research activity in Prof. Mukerjee's group is an interdisciplinary approach encompassing the areas of solid state chemistry, spectroscopy, and electrochemistry of electrode materials for electrochemical energy conversion and storage. The current focus is targeted towards technologies for proton exchange membrane (PEM) fuel cells and for batteries, encompassing electrocatalysis of oxygen reduction, CO tolerance and methanol oxidation reactions, elevated temperature polymer electrolyte membranes, advanced rechargeable batteries with nickel metal hydrides and lithium insertion electrodes for lithium ion and lithium polymer batteries.

Dario R. Dekel is an Associate Professor of Chemical Engineering Department at Technion, Israel Institute of Technology. Prof. Dekel investigates novel cutting-edge materials and processes for the development of advanced electrochemical devices, such as novel fuel cells, as well as other technologies for energy storage and generation. Prof. Dekel's current focus involves research of anion conducting ionomeric materials, non-PGM electrocatalysts, anion exchange membranes, anion transport through electrochemical cells, and fuel cells. Dekel's research team is one of the few groups worldwide leading the research on materials design for anion exchange membrane fuel cell technology.